Journal of Materials Chemistry A

Accepted Manuscript

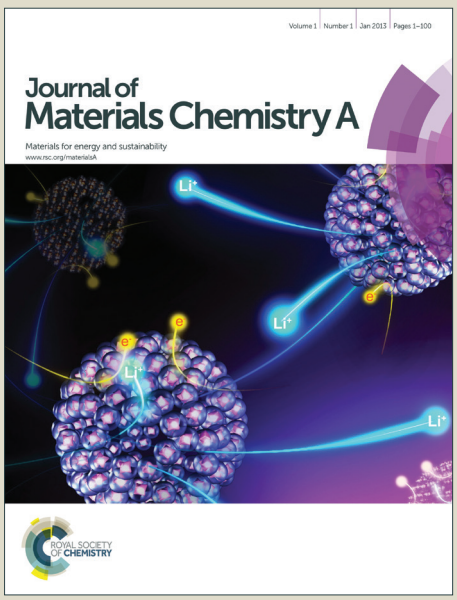

ROYAL SOCIETY OF CHEMISTRY

www.rsc.org/materialsA

Journal Name

RSCPublishing

ARTICLE

Spectroelectrochemical Investigation of Redox States in a Polypyrrole/Lignin Composite Electrode Material

Cite this: DOI: 10.1039/x0xx00000x

Received 00th January 2012,
Accepted 00th January 2012

DOI: 10.1039/x0xx00000x

www.rsc.org/

F. N. Ajjan †,[a], M. J. Jafari †,[b], T. Rębiś[c], T. Ederth[b] and O. Inganäs*.

We report spectroelectrochemical studies to investigate the charge storage mechanism of composite polypyrrole/lignin electrodes. Renewable bioorganic electrode materials were produced by electropolymerization of pyrrole in the presence of a water-soluble lignin derivative acting as dopant. The resulting composite exhibited enhanced charge storage abilities due to a lignin-based faradaic processes, which was expressed after repeated electrochemical redox of the material. The in-situ FTIR spectroelectrochemistry results show the formation of quinone groups, and the reversible oxidation-reduction of these groups during charge-discharge experiments in the electrode materials. The most significant IR bands include carbonyl absorption near 1705 cm^{-1}, which is attributed to the creation of quinone moieties during oxidation, and absorption at 1045 cm^{-1} which is due to hydroquinone moieties.

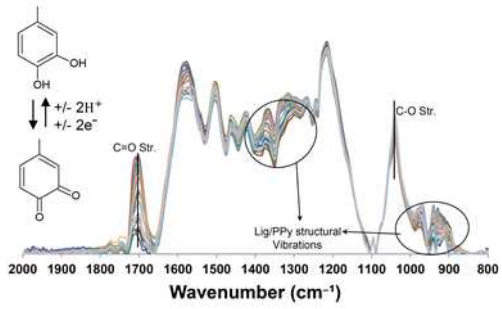

1 Introduction

The need for new materials and systems for charge storage is a consequence of the rapidly growing supply of intermittent wind and solar electricity. The ability to effectively store electrical energy through electrochemical and double layer processes is becoming crucial. In order to obtain high charge capacity and specific capacitance, and thus good energy and power density performances, new materials may be needed. Thus, a resurgence of research on batteries and supercapacitors is visible.[1,2]

One of the strategies is the preparation of novel redox polymer and conjugated polymer-based electrode materials.[3–89] Electronically conducting polymers were intensively studied after the discovery of metallic polyacetylene by Shirakawa, McDiarmid, Heeger, et al.[10] A strong interest in the development of new storage devices emerged at this time. The benefits of conductive polymers are their high electrical conductivity, processability, low cost and electrochemical reversibility. This is due to the presence of fast charge transfer in the polymeric chain, associated with intercalation/deintercalation of counter-ions during the redox process.[11,12] For many of these reasons, polypyrrole (PPy) seems to be a good candidate for this purpose, as one of the more stable materials, with relatively high theoretical specific capacity 75 mAh g^{-1} (with dopant) and a specific energy density ranging from 80 to 390 Wh kg^{-1}.[13,14] However, PPy doped by small, mobile counteranions such as perchlorates, still suffer from self-discharge, from insufficient charge storage density compared to inorganic materials used in secondary batteries,

† These authors contributed equally to this work.

and also undergo geometrical changes, which limits the long-time cycling of the electrode.

A feasible strategy to improve the performance of organic energy storage devices would be to use electroactive macromolecular compounds with a redox-reactive dopant behavior, to create a composite electrode material to enhance the properties of the electroactive compound. There is a resurgent interest in the use of biopolymers such as cellulose or lignin derivatives in the development of electrochemical devices.[15–20] Both biopolymers are renewable and abundant, and accessible as the main or side product of existing industries. Their abundance and low cost form their attractiveness from the economical point of view. Taking into account electrochemical demands, particularly in the field of energy storage, but also for sensor applications and electrocatalytic properties, lignin derivatives seem to be especially attractive. Lignin contains three monolignols, the p-hydroxyphenol (H), guaiacyl (G), and syringyl (S) units. The amount and composition of H, G, and S in lignins vary among taxa, cell types, and individual cell wall layers and also with environmental conditions.[21] Lignosulfonates are water soluble by-products of the pulp and paper industry, and were recently used as electroactive materials and showed strong electrocatalytic behavior toward biomolecules.[22,23] This activity is attributed to the existence of many phenolic and methoxy phenolic functional groups that can be easily converted into reversible quinone/hydroquinone redox moieties. Furthermore, lignosulfonates have negatively charged sulfonic groups, may be treated as polyanions and can be used as dopants for conducting polymers.

The current study is based on recent work[11] where we showed the composite of lignin with PPy as an electroactive interpenetrating network, with both PPy and lignin contributing to the redox activity at two different potentials. We have shown that a quinone/hydroquinone redox species is causing the added redox wave in this composite material. The hypothesis is that the monolignols in the composite material can be oxidized to quinone, which are later used in reversible redox. We therefore aim to characterize the composite material with *ex-situ* and *in-situ* infrared (IR) spectroscopic techniques.[24,25]

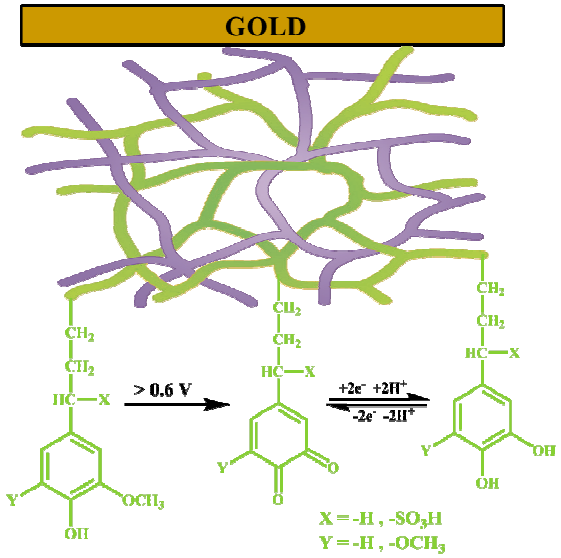

Scheme 1. Schematic representation of the interpenetrating network of PPy/Lig biocomposite formed on a gold substrate by electrochemical polymerization of pyrrole in the presence of lignosulfonate. Green lines represent lignin with the redox e^-/H^+ exchange reaction and the purple lines represent PPy.

Spectroscopic methods have been used to characterize the doping level, the conjugation length, and the electronic structure of conducting polymers.[26–29] Among these, polypyrrole has been studied extensively; in particular, several publications concern *ex situ,*[30–32] or *in situ* Raman[33] and infrared studies of film structure in response to redox cycling and overoxidation,[28,34] doping,[33] or degradation.[35] The power of *in-situ* spectroelectrochemical Fourier-transform infrared (FTIR) spectroscopy is in the direct observation of structural and electronic changes taking place during electrochemical reactions, due to changes between different oxidation states. Experiments are performed on polymer films coating the surface of electrodes in the presence of electrolyte, with spectra recorded in the mid-IR and the near-IR ranges. Experimental developments have been accompanied by calculations of vibrational spectra,[36,37] where, for example, Tian and Zerbi [38,39] investigated spectra of reduced and oxidized forms of polypyrrole, suggesting benzoid structure of reduced and quinoid structure of oxidized polypyrrole. Due to the structural diversity of lignins, efforts concerning the IR spectroscopy of lignins have been concentrated on identification of spectral features of lignin constituents, and to use this information for investigation and identification of lignin varieties, in particular with regard to source species.[40,41]

2 Experimental Section

2.1 Electrode Preparation.

The electroactive interpenetrating network of polypyrrole/lignin (PPy/Lig) composite was prepared by galvanostatic electropolymerization of 5 g L^{-1} freshly distilled pyrrole (Py, Aldrich) monomer from an aqueous-acidic solution of 0.1 M

$HClO_4$ (Merck), containing different concentrations (1.7, 5.0, 7.5, and 15 g L^{-1}) of lignin derivative in the form of lignosulfonates (LC30, M_w=13400, MeadWestvaco). The polypyrrole film was electrodeposited in the same manner as the PPy/Lig composite but without lignin (Figure S1). The three-electrode configuration used for the synthesis and characterization of interpenetrating networks was based on a gold disc electrode of 0.07 cm^2 geometrical area as a working electrode, Ag/AgCl as a reference electrode (both Bioanalytical Systems Inc. USA), and a large surface area Pt as counter electrode. By applying a constant current density of 0.25 mA cm^{-2} for 300 s (75 mC cm^{-2} total charge), the PPy/Lig composite thin film was generated uniformly onto the different Au surfaces. For *ex-situ* experiments, 1000 Å thick gold was evaporated onto a silicon wafer using 20 Å thick titanium as adhesive layer. For *in-situ* experiments, 2000 Å of gold was evaporated onto Fisherbrand QT200 filter paper (Fisher Scientific).

The electrode was rinsed with deionized water and transferred to a fresh solution of 0.1 M $HClO_4$ electrolyte. Then, cyclic voltammetry (CV) was performed to generate quinone moieties from the lignosulfonate polymer within the potential range between -0.2 V and 0.7 V vs Ag/AgCl by applying 25 cycles at 100 mV s^{-1}. The development of the quinone moieties was clearly shown by following the first three cycles in Figure S3. In other experiments, overoxidation of the composite was generated by applying potentials from -0.2 V to 1.5 V. MilliQ (Millipore) water was used in all the experiments.

2.2 Electrochemical quartz crystal microbalance (EQCM).

Quartz crystal microbalance studies were performed with a Q-Sense E4 instrument using gold-coated quartz crystals in an open cell module. PPy/Lig composites were galvanostatically deposited using an Autolab PGStat 10 (Eco Chemie, the Netherlands) from a solution consisting of different concentrations (Table 1) of pyrrole and lignin, after a waiting time of 5 minutes in the polymerization solution to get a stable background. The frequency change was monitored during deposition of the PPy/Lig composite and analysed using the Sauerbrey equation to deduce the mass.

2.3 Spectroelectrochemical Characterization.

Ex-situ Fourier-transform Infrared Reflection-Absorption Spectroscopy (IRAS) measurements were performed at 85° grazing angle in a Bruker IFS66 spectrometer with a LN_2-cooled MCT detector. The optical bench was continuously purged with nitrogen during the measurements. IR spectra were acquired at 2 cm^{-1} resolution and 3000 scans between 4000 and 800 cm^{-1}. Background spectra were obtained using an uncoated gold substrate.

Attenuated Total Reflectance-FTIR (ATR-FTIR) spectroscopy was combined with CV measurements for *in-situ* monitoring of the electrochemical process. **Scheme 2** shows the schematic view of the cell for measurements. Measurements were carried out with a PIKE MIRacle ATR accessory with a diamond prism in a Vertex 70 spectrometer (Bruker) using a DTGS detector at room temperature, and the system was continuously purged with N_2. IR spectra were acquired at 4 cm^{-1} resolution and 32 scans between 4000 and 800 cm^{-1}. Background spectra were from the gold-coated filter paper substrate in electrolyte environment. The cyclic voltammograms were measured at a scan rate of 1 mV/s and IR spectra were recorded at 23 potentials from a starting potential of -0.4 V up to 0.8 V in forward and backward CV cycle scan modes. Each IR spectrum was recorded over a duration of 20 sec, and successive measurements were performed at 0.1 V intervals with an accuracy of ±20 mV at 25 °C. Presented spectra are baseline-corrected by subtraction of a linear baseline extending over the spectral ranges presented in the figures.

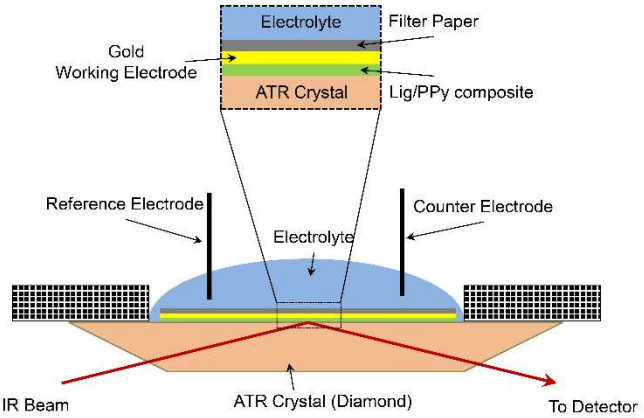

Scheme 2. Schematic representation of the *in-situ* ATR-FTIR setup for spectroelectrochemical investigation of the PPy/Lig composite redox process. Working, counter and reference electrodes are depicted, as well as the active material (the PPy/Lig composite) deposited on the gold-coated filter paper in contact with the electrolyte solution.

2.4 Absorbance Spectroscopy.

Absorption measurements were acquired by using an Ocean Optics UV–vis spectrophotometer model USB4000 with a thin-layer quartz cuvette and gauze Au working electrode, Ag/AgCl as a reference electrode (both Bioanalytical Systems Inc. USA), and Pt as counter electrode.

3 Results and Discussion

3.1 *Ex situ* spectroelectrochemical measurements.

The electrochemical measurements were initially performed in the -0.2 to 0.7 V potential range by CV, to follow the behavior of the polypyrrole/lignin (PPy/Lig) composite. The cyclic voltammogram of PPy/Lig (Figure 1A) shows quasi-reversible redox peaks that correspond to the quinone moieties with the formal potential E'^0 of 0.57 V *vs.* Ag/AgCl in acid solution, originating from monolignol precursors contained in lignin. Unlike PPy/Lig, PPy/ClO_4^- gives a capacitive-like rectangular

voltammogram with no pronounced peaks, suggesting only fast insertion/withdrawal of the anion ClO_4^- into/from the polymer. The incorporation of lignin strongly contributes to the total capacity of this system due to additional faradaic reaction. To maximize charge storage, our purpose is to incorporate the optimum amount of lignin inside the composite. Thus, the strategy of preparation of the composite from electrolyte solution containing different biopolymer/pyrrole mass ratios (0.34:1; 1:1; 1.5:1; 3:1) was applied in the broad range of lignin concentrations 1.7-15 mg/ml. Composites comprising different concentrations of lignin were synthesized and the influence of biopolymer/pyrrole ratio on the total charge storage performance was evaluated, as depicted in Figure 1B. The voltammograms at different concentrations shows different faradaic activity in the lignin region (0.4 to 0.7 V). However, in the potential region of PPy (-0.2 to 0.3 V) there were no changes, as PPy can be sufficiently doped by ClO_4^- independently of lignin concentration. Interestingly, the influence of electrolyte solution composition on the final mass of the composite was rather minor, as shown in the results summarized in Table 1. However, different concentrations of Lig/Py solutions can slightly affect the total performance of the resulting PPy/Lig composite. Changes were only observed in the potential range of faradaic peaks where the quinone/hydroquinone activity is observed. Results indicate that there was an improvement of up to 20% of the total capacity, reaching an optimum at the biopolymer/pyrrole mass ratio at 1.5:1.

Table 1. Experimental data of lignin/pyrrole mass ratio (Lig/Py), moles (n_{Py} and n_{Lig}) and concentration of reactants (C_{Py} and C_{Lig}), mass of the PPy/Lig composite (m_{comp}) obtained by EQCM measurements and capacity values (Q) for the biocomposite material at varying Lig/Py ratios.

Lig/Py ratio	n_{Py} [mol]	C_{Py} [mol L^{-1}]	n_{Lig} [mol]	C_{Lig} [mol L^{-1}]	m_{comp} [µg cm^{-2}]	Q [mA h g^{-1}]	Yield [mg C^{-1}]
0.34	$2.98 \cdot 10^{-4}$	$7.45 \cdot 10^{-2}$	$1.19 \cdot 10^{-7}$	$2.98 \cdot 10^{-5}$	53	60	0.70
1	$2.98 \cdot 10^{-4}$	$7.45 \cdot 10^{-2}$	$3.50 \cdot 10^{-7}$	$8.77 \cdot 10^{-5}$	54	67	0.72
1.5	$2.98 \cdot 10^{-4}$	$7.45 \cdot 10^{-2}$	$5.26 \cdot 10^{-7}$	$1.31 \cdot 10^{-4}$	49	72	0.65
3	$2.98 \cdot 10^{-4}$	$7.45 \cdot 10^{-2}$	$10.52 \cdot 10^{-7}$	$2.62 \cdot 10^{-4}$	47	66	0.63
Pure Py [11]	$2.98 \cdot 10^{-4}$	$7.45 \cdot 10^{-2}$	-	-	25	30	0.30

From the galvanostatic charge-discharge experiments of these electrodes, the variation of the capacity from 60 to 72 mAh g^{-1} confirmed that this behavior was comparable with the corresponding cyclic voltammograms (Figure 1b,c).

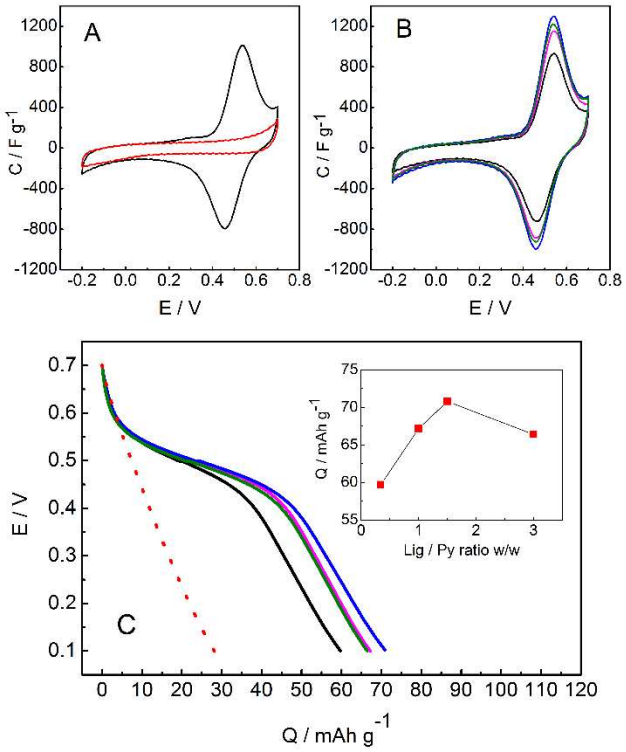

Figure 1. Results for PPy/Lig composite: cyclic voltammograms of (A) PPy (red line) and PPy/Lig (black line); (B) PPy/Lig composite at different lignin/pyrrole mass ratio 0.34:1 (black line); 1:1 (pink line); 1.5:1 (blue line); 3:1 (green line) mass ratio in 0.1M $HClO_4$ solution. Scan rate: 100 mV s^{-1}; (C) discharge curves of PPy/ClO_4^- (red dashed line) and PPy/Lig composite at different concentrations of lignin at 1 A g^{-1} different concentrations. Insert: Dependence of the total capacity as function of the lignin/pyrrole mass ratio.

The *ex-situ* IRAS spectra of lignin, PPy and their composites in the 2000-800 cm^{-1} region are shown in Figure 2. For lignin (the top spectrum), the broad shoulder around 1680 cm^{-1} corresponds to C=O stretching in a conjugated carbonyl.[42] Bands at 1599 and 1504 cm^{-1} are due to aromatic ring skeletal vibrations, and bands at 1464, 1452 and 1427 cm^{-1} are attributed to aromatic skeletal vibrations combined with methyl and methylene C-H deformations.[41] A weak band near 1369 cm^{-1} can be assigned to aromatic skeletal vibration combined with C-H in-plane deformation of syringyl (S) and guaiacyl (G) units.[43] The spectrum of lignin also shows a strong band at 1267 cm^{-1} with a shoulder at 1304 cm^{-1}, which correspond to aryl ring breathing with C=O and C-O stretch of GS lignin,[44] respectively. A very strong peak at 1230 cm^{-1} is observed, which is attributed to C-C and C-O stretching vibrations in lignin combined with aromatic ring stretching modes.[45] The band near 1150 cm^{-1} is attributed to aromatic C-H in-plane deformations, characteristic of lignin.[44] The peak at 1083 cm^{-1} with shoulders at 1096 and 1088 cm^{-1} is attributed to out-of-plane stretching of phenols and C-O deformation of secondary alcohol and aliphatic ether.[40] The peak at 1050 cm^{-1} can be due to C-O stretch of aryl-O-CH_3 and aryl-OH of GS lignin[46], skeletal vibrations of aromatic units, or C-H and C-O

deformations, and have been associated also with other modes,[40,41] but it is difficult to distinguish them from each other. Also sulfonates are expected to contribute to this peak, see below. Weak peaks near 943 and 856 cm^{-1} are due to C-H aromatic ring deformations of GS lignin, with that at 860 cm^{-1} perhaps also combined with aromatic skeletal deformation.[44] Overlapping with the bands originating from the lignols, we expect to find contributions from the sulfonate groups. S-O and S=O vibrations in SO_3^- are typically intense in IR spectra due to the polarity of the bonds. The mass of the S atom and weak electronic coupling with the surroundings also makes their positions rather insensitive to the structural environment, but it will vary with the counterion in a salt. For sodium salts, bands at 1060-1050 and 1190-1170 cm^{-1} are expected.[47] In the spectrum, a shoulder near 1190 cm^{-1} is present, but the moderate intensity of the absorption around 1050 cm^{-1} (which is also expected to have other contributions as explained above) and the weak shoulder around 1190 cm^{-1}, suggest that the degree of sulfonation in the lignin is low.

Peak assignment in polypyrrole spectra from literature data is complicated by the variations in peak positions and intensities obtained on samples prepared with different methods, variations with oxidation and doping levels, conjugation lengths,[30,36,48,49] and the ratio of polaron/bipolaron excitation.[28] It is of note, though, that spectra of doped PPy tend to be similar, while those of undoped PPy vary considerably with preparation procedures.[38,50] The high-frequency region (>2000 cm^{-1}, not shown) of the spectra for PPy and the composites in Figure 2 is dominated by a progressive, but largely featureless, increase in absorbance with wavenumber, characteristic of doped PPy,[39,50] and caused by excitation of free charge carriers,[28] almost completely obscuring the contributions from stretching of N-H (around 3400 cm^{-1}) and C-H (around 3100 cm^{-1} for aromatic C carbons and 2900 cm^{-1} for alkyl carbons).

Further, in the spectrum of polypyrrole, a very weak band at 1722 cm^{-1} arises from C=O stretching as a result of the oxidation of polypyrrole during polymerization.[51] Peaks and shoulders at 1585, 1543, 1478 and 1450 cm^{-1} are due to C=C stretch and other characteristic vibrations of the pyrrole aromatic ring.[37] The band at 1299 cm^{-1} is attributed to C-N in-plane deformation,[52] while the shoulder near 1360 cm^{-1} can correspond to C-N stretch with C-C vibration. Bands at 1215, 1155, 1083 and 1045 cm^{-1} can be assigned to C-C-C and C-N-H bending, C-N stretch and N-H deformation as typical aromatic ring vibrations of polypyrrole.[53] The band at 969 cm^{-1} is attributed to C=C-C in-plane and out-of-plane deformation,[37] and bands at 945 and 884 cm^{-1} indicate C-H in-plane deformation and C-H out-of-plane bending, respectively, other vibrations at lower frequencies (shoulders at 876 and 836 cm^{-1}) are caused by different C-H vibrations.[54]

The IR spectra of three PPy/Lig composites (Figure 2) prepared from solution compositions ranging from 3:1 to 1:3, yield small differences in the resulting spectra. Notable features in these are intense bands emerging at 1570-1580 and 940 cm^{-1}, suppression of the lignin absorptions at 1510 and 1450, 1270, 1150 and 1080 cm^{-1}, relative enhancements of the broad PPy band around 1300 cm^{-1} and of the carbonyl band at 1715 cm^{-1}. Overall, the peak patterns of the composite spectra are similar to a blue-shifted PPy spectrum. The suppression of features from the lignin spectrum is in agreement with observations that in a composite between a conducting and a non-conducting polymer, the spectrum of the conducting material tends to mask the non-conducting, and in particular spectral features associated with aromatic moieties will be enhanced and dominate the composite spectrum.[55,56] This enhancement, caused by conduction charges, is related to the overall intensity enhancement of the composite as a result of coupling of the vibrational modes with the electronic states of the increasingly abundant charge carriers upon doping.[57] Considering the spectral features of the composite in more detail, we first note that the appearance of the carbonyl mode at 1716 cm^{-1} after polymerization indicates oxidation and decomposition of GS monolignol.[58] The band at 1575 cm^{-1} indicates C=C stretch and weak peaks in the 1500-1400 cm^{-1} region correspond to aromatic ring vibrations. The 1400-1100 cm^{-1} region contains bands and shoulders from overlap of aromatic skeletal and various deformation modes. The spectral changes upon doping, as well as the shift in relative intensities of the PPy and lignin contributions, makes assignments uncertain at this stage. However, possible contributions are aromatic skeletal vibration combined with C-H in-plane deformation (1370 cm^{-1}) and C-O stretch (1302 cm^{-1}) of GS lignin, with C-N deformation and C-C vibration (1320 cm^{-1}) of polypyrrole.[37] The strong band at 1225 cm^{-1} is due to C-C stretch with C-O vibration of lignin, and shoulders indicate C-O and C=O stretch of GS lignin covered by C-C-C bending in the PPy backbone (1250 cm^{-1}) and polypyrrole ring vibrations (1170 cm^{-1}). Lignin (1050 cm^{-1}) and polypyrrole (1045 cm^{-1}) amalgamate into a band at higher frequency (1055 cm^{-1}). If not an effect of the doping of the composite, this shift could be caused by phenol vibrations and C-O deformation in lignin during polymerization, with additional contribution from lignin sulfonate. Bands below 1000 cm^{-1} are associated with C=C-C vibrations of polypyrrole (971 cm^{-1}) and different C-H vibration of HGS lignin and polypyrrole (band at 941 cm^{-1} and shoulders at lower 900 cm^{-1}).[37] The new intense band appearing at 941 cm^{-1} is tentatively attributed to shift and overlap of different C-H deformations in PPy (945 and 884 cm^{-1}) and lignin (943 and 856 cm^{-1}), in combination with the aforementioned enhancement of PPy spectral features. Possible contributions to this band in the composite include shifts due to ring interactions, such as π–π stacking, differences in orientation of the PPy in the composites and the pure PPy film, or oxidation of the lignin, though a discrimination between these is difficult.

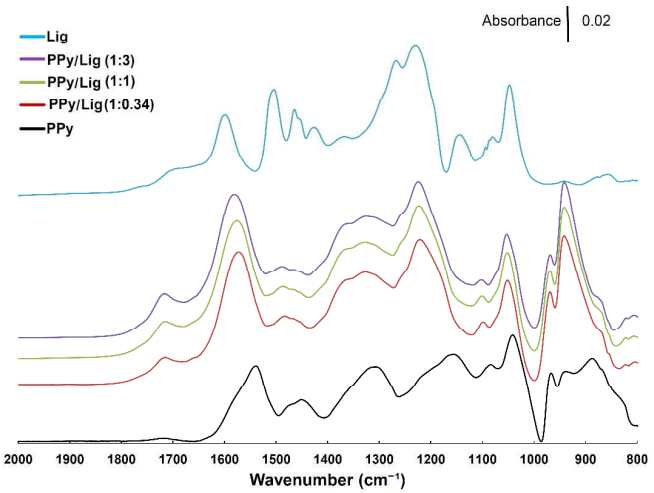

Figure 2. Ex-situ IRAS spectra of lignin (blue), polypyrrole (black) and PPy/Lig composites at different lignin/pyrrole mass ratio, 3:1 (purple), 1:1 (green), and 0.34:1 (red).

3.2 Redox stability and overoxidation.

One of the most important figures of merit for energy storage devices is to achieve very many charge/discharge cycles. For this purpose, we analyzed the behavior of the PPy/ClO_4^- and PPy/Lig composites after 1000 cycles within the potential range of -0.2 to 0.7 V, considering this electroactive potential region as a proper one for a future device. In the case of PPy/Lig composite, we observed a strong decrease in charge capacity after 1000 cycles (Figure 3a). Interestingly, PPy/ClO_4^- exhibits stronger resistance to cycling (Figure 3b). PPy/Lig composites showed large loss of quinone redox. Redox activity may decrease due to the destruction of the guayacil units (G) of lignin after cycling, after which mainly the syringyl units (S) remain. This behavior may be tentatively explained by possible breakages of covalent bonds or possible nucleophilic attack on the quinone groups.

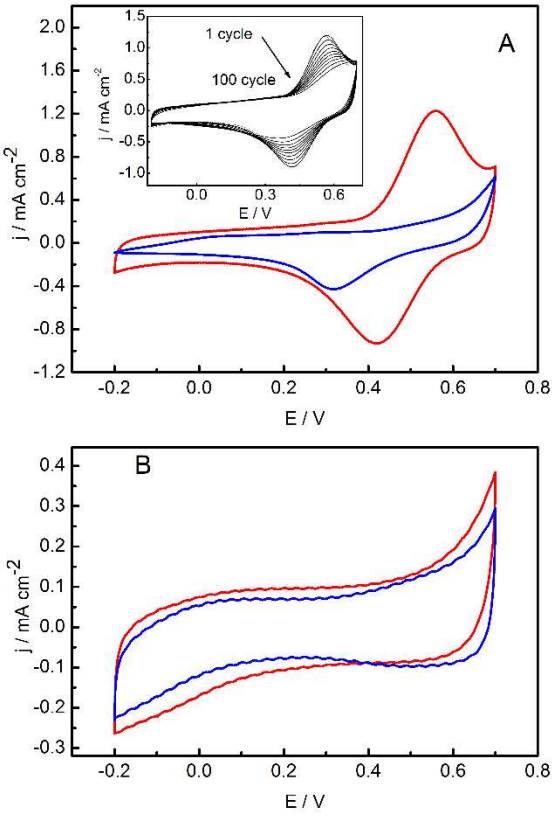

Figure 3. (A) Cyclic voltammetry of the PPy/Lig composite before 1000 cycles (red line) and after 1000 cycles (blue line) within potential range of -0.2 to 0.7 V. The inset shows the cyclic voltammograms of PPy/Lig recorded during first 100 cycles (every 10 cycles). Scan rate 100 mV s^{-1}. (B) Cyclic voltammetry of PPy/ClO_4^- before 1000 cycles (red line) and after 1000 cycles (blue line) within potential range of -0.2 to 0.7 V. Scan rate: 100 mV s^{-1}.

In order to understand the loss of electroactive capacity, electrochemical overoxidation of PPy/ClO_4^- to PPy/ClO_4^- and PPy/Lig to OPPy/Lig composites was performed by cyclic voltammetry within the potential range of -0.2 V to 1.5 V (Figure 4 and 5). Figure 4 shows that the OPPy/ClO_4^- show different behavior with respect to PPy/ClO_4^- after several cycles of cyclic voltammetry. The comparison between the voltammograms of PPy/ClO_4^- before and after overoxidation prove that loss of electroactivity and increase of resistivity is observed after overoxidation of PPy/ClO_4^-. In Figure 5, the cyclic voltammetry of OPPy/Lig composite was entirely irreversible. The overoxidation peak of the PPy/Lig composite appeared at about 0.9 V (green line) and through the reverse scans from positive to negative potential we observed the total lack of electroactivity (blue line). Thus the overoxidation of PPy/Lig composite shows that the biocomposite is also sensitive to overoxidation.

As was suggested previously[59,60] overoxidation depends on several factors such as the pH of the electrolyte solution and polarization potential. Moreover, the overoxidation potential of 1.5 V matches the water decomposition potential giving rise to intermediate species (O_2, H_2O_2, OH•). Most likely the influence of the O_2 is not responsible for the overoxidation of the doped PPy/ClO_4^-. However, hydroxyl radicals[61] lead to this

irreversible process generating carbonyl groups at β–C of pyrrole units of PPy. This is clearly shown in the increased intensity and shift of the carbonyl absorbance to 1720 cm^{-1} in the IR spectrum after overoxidation (see below). In addition, hydroxyl radicals affect lignin structure as they might react with lignin units, thus causing a loss in their electroactivity.

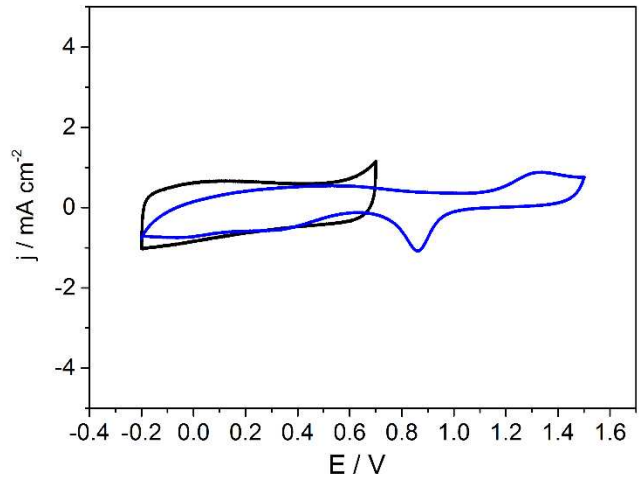

Figure 4. Cyclic voltammogram of PPy/ClO_4^- before overoxidation (black line) within potential range of -0.2 to 0.7 V and after overoxidation (blue line) within potential range of -0.2 to 1.5 V. Scan rate: 100 mV s^{-1}.

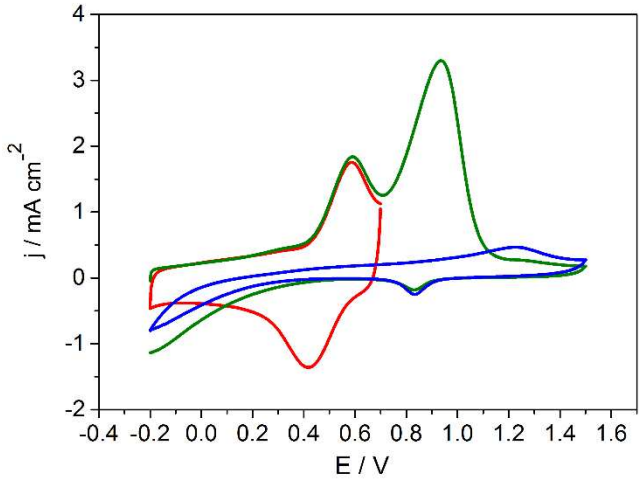

Figure 5. Cyclic voltammograms of PPy/Lig (red line) within potential range of -0.2 to 0.7 V, and overoxidation process of PPy/Lig after the first cycle (green line) and after the 5 cycles (blue line) within potential range of -0.2 to 1.5 V. Scan rate: 100 mV s^{-1}.

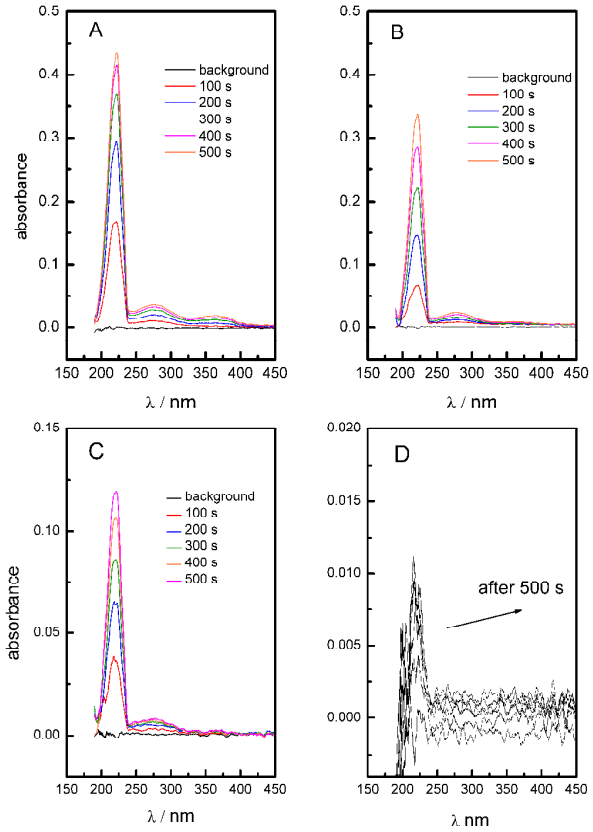

Figure 6. UV – Vis spectra of 0.1M $HClO_4$ electrolyte solution with polarization of PPy/Lig composite electrode at applied constant potential of 0.8 V (A), 0.7 V (C) and 0.6 V (D) during several polarization time. (B) UV – Vis spectra of 0.1M $HClO_4$ electrolyte solution with polarization of PPy/ClO_4^- electrode at 0.8 V.

Moreover, PPy is known to undergo degradation when the anodic potential is greater than 0.6 V [62–64]. This is due to the formation of maleimide during the oxidation, thus degrading the PPy. We also observed the same effect when the anodic potential is greater than 0.6 V. We recorded the UV-VIS spectrum of the electrolyte during experiments, and find the signature of maleimide at 200-300 nm. When the PPy/Lig composite was polarized at 0.6 V for different times, no characteristic UV-Vis peak is observed from the electrolyte (Figure 6). However, when the polarization potential was 0.7 V and 0.8 V respectively, a maximum absorption peak at (λ_{max}) 222 nm becomes visible and increase with time and potential.

Changes in the spectrum of PPy/Lig composites upon oxidation from the reduced state are shown in Figure 7, accompanied by spectra of the composites after 1000 redox cycles (1000 CV) and after overoxidation. There are a few striking features of this set: the overall increase in intensity with oxidation, the considerable increase of the C=O band intensity at 1715 cm^{-1}, and the irregular intensity variations of the 1097, 1051, 969, and 941 cm^{-1} bands. The increasing similarity of the composite to the PPy spectrum upon increased oxidation, and

the significant increase in total intensity of the spectrum upon overoxidation, results from the electronic-vibrational enhancement with the number of charge carriers in the composite, increasing the relative contribution from PPy to the spectrum, as was discussed above. To better understand the cause of the spectral changes, it is informative to monitor the changes in peak positions for the four spectra in Figure 7, since this gives an indication of which bands participate in conversions upon redox cycling, see Table 2.

Table 2. Peak positions for the spectra in Figure 7. The "shift" column indicates the difference between the highest and the lowest wavenumber for each absorption peak.

Reduced (cm^{-1})	Oxidized (cm^{-1})	Cycled (cm^{-1})	Over-oxidized (cm^{-1})	Shift (cm^{-1})	Assignment
1715	1717	1721	1719	6	C=O stretch
1565	1577	1587	1582	22	C=C and aromatic ring skeletal vibrations
1482	1486	1498	1488	16	Monolignol ring vibrations Monolignol ring vibrations
1468	1467	1466	1468	2	
1452	1452	1450	1448	2	Monolignol ring vibrations
1325	1329	1311	1324	18	Several PPy ring vibrational modes.
1219	1225	1226	1223	7	C-C and C-O stretch in lignin with C-N stretch and N-H in-plane bending in PPy
1097	1101	1101	1102	4	PPy ring mode
1046	1049	1051	1051	5	C-O stretch of aryl-O-CH_3 and aryl-OH overlapped with N-H deformation.
969	970	969	968	2	C-H out-of-plane deformation
941	942	942	940	2	C-H out-of-plane deformation

Comparing the locations of the peak positions in the four spectra, it is clear that some positions are nearly unaffected and change very little (2-4 cm^{-1}) by the redox cycling, while others are substantially shifted (~20 cm^{-1}). The latter absorptions are related to functional groups or structural features that are involved in, or attached to groups participating in, the chemical conversion upon oxidation or cycling. Assignment of these bands should give a clearer picture of the processes occurring upon redox cycling of the PPy/Lig composite.

The intensity of the carbonyl band at 1715 cm^{-1} increases significantly with the oxidation level (see inset of figure 7), and is also slightly shifted to higher frequencies, ending at 1721 cm^{-1} for the 1000 times cycled sample, indicating loss of conjugation (the location of the band indicates presence of conjugated carbonyls, related to the hydroquinone/quinone reactions of GS lignols, as explained above). In polypyrroles, this absorption has also been attributed to formation of carbonyl groups at the pyrrole ring β-position upon overoxidation.[33] The oxidized forms also have a very weak shoulder near 1660 cm^{-1}, suggesting the presence of other conjugated carbonyls, possibly amides. The intense band at 1565 cm^{-1}, originating in C=C stretching and ring modes, has the largest shift of the absorptions, demonstrating that functional groups attached to the rings play an important role in the redox conversion. The blue-shift for the oxidized and 1000 time cycled forms is associated with conversion from the benzoid to quinoid ring structures in lignols. Comparing the peak positions of the cycled, over-oxidized and oxidized samples in Table 2, we find that the cycled sample overall has larger shifts compared to the overoxidized, showing that the cycling causes greater structural changes than overoxidation. While both processes lead to loss of electroactivity, the clear differences in the infrared spectra are evidence that the chemical changes reducing the redox capacity are different in the two cases. These changes are also visible for the ring skeletal vibrations (1482 cm^{-1}) and PPy ring vibrations (1325 cm^{-1}). This is consistent due to the loss of conductivity upon disrupted conjugation, which is expected after overoxidation. The relative intensities (Figure 7 inset) of the 1715 cm^{-1} vibration show that there are no significant differences between overoxidized and 1000 time cycled forms. This signal is due both to quinones from the lignin and from overoxidized polypyrrole.

The considerable differences in the shifts of the three aromatic ring skeletal vibrations around 1480-1450, originating from monolignols, reflect the distribution between S, G and H monolignols. The large shift of the vibration at 1482 cm^{-1} suggests that this may represent the S, G monolignols, while the smaller shifts at 1468 and 1452 cm^{-1} can be associated to H monolignols, which do not participate in the redox reactions.

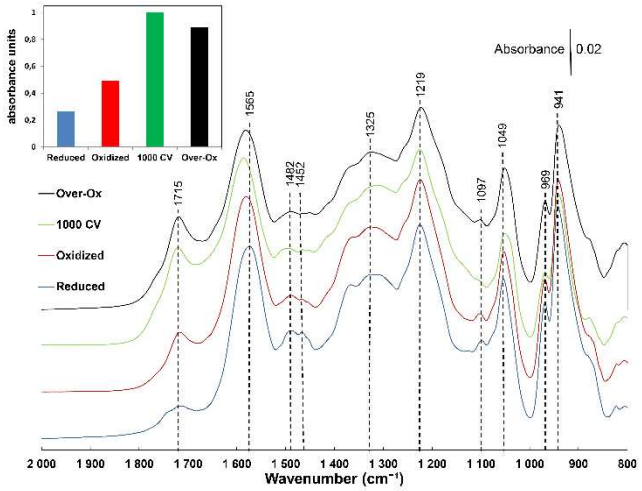

Figure 7. *Ex-situ* FTIR spectra of 1:1 PPy/Lig composite films in the reduced and oxidized forms, after 1000 cycles of CV, and after overoxidation. The inset shows relative intensities of the C=O band at 1715 cm^{-1} of the PPy/Lig composite in different oxidation states.

3.3 *In-situ* spectroelectrochemical measurements.

Cyclic voltammetry experiments for *in-situ* spectroelectrochemical measurements were also conducted, starting from the potential of -0.4 V up to 0.8 V and back to -0.4 V, in order to follow spectral changes in the composite during redox. Spectra were collected at 0.1 V potential intervals at 1 mV s^{-1} scan rate.

The *in-situ* FTIR-ATR spectra of a PPy/Lig composite at different potentials during voltammetric cycling are given in Figure 8. Figure 9 shows the difference spectra of the composite at different applied potentials, obtained by subtracting the spectrum of the pristine sample from each measured spectrum. Bands at 1706 and 1043 cm^{-1} are due to C=O and C-O stretching in lignin, respectively, and upon hydroquinone/quinone conversion, the intensity of one of them increases, while the intensity of the other decreases. The same behavior is also seen for the bands at 933 and 906 cm^{-1}, corresponding to C-H out-of-plane deformation of lignin, but associated to aromatic/non-aromatic ring vibrations.[40] Bands at 1593 and 1361 cm^{-1} are related to C=C and structural ring vibrations of lignin and polypyrrole and show skeletal changes in the structure of the material during the *in-situ* experiments.
As the applied potential goes positive (oxidation), a band around 1706 cm^{-1} (C=O stretch) appears and its intensity increases as the applied potential becomes more positive. This band then disappears when the applied potential becomes negative (reduction). The intensity of the band at 1043 cm^{-1} (C-O stretch of aryl-O-CH_3 and aryl-OH of GS lignin) decrease with oxidation, while it increases again upon reduction. The potential dependence of the C=O and C-O band intensities are presented in Figure 10a.

The normalized intensity of the C=O band does not show any significant change in the region from -0.4 to -0.1 V and starts to increase at potentials around -0.1 V, reaching a maximum at 0.8 V in the forward scan. In the backward scan, the intensity of the C=O band decreases and returns to near the initial state at -0.4 V, thus showing reversible behavior. The C-O band shows an opposite trend, with an intensity maximum at -0.4 V. The conversion between the C=O and C-O bands of GS lignin during the redox process demonstrates the reversible quinone/hydroquinone reaction in the PPy/Lig composite.[11] Figure 10b shows other structural vibrational changes of lignin during the redox process; the normalized intensity of C-H out-of-plane bending vibration at 902 cm^{-1} [4] decreases following an increase in the applied potential, while the intensity of the band related to C-H in-plane deformation at 933 cm^{-1} increases with the potential.[65]

Interestingly, the IR spectra highlight the predominance of the C-H out-of-plane bending mode in the aromatic hydroquinone ring (reduced state) and the prevalence of the C-H in-plane deformation in the non-aromatic quinone (oxidized state). A plausible explanation of this experimental observation could be sought in a variation of the extinction coefficient of the out-of-plane and in-plane deformations of the C-H bond associated, respectively, with the hydroquinone and the quinone forms, which causes the observed inversions in the intensity of the resulting absorbances. However, a detailed analysis and calculation of the extinction coefficients is beyond the scope of this work.

The hydroquinone/quinone conversion can also be demonstrated by changes in skeletal vibrations of lignin. Figure 11 shows a change of position and normalized intensity of the peak which is due to aromatic ring vibrations of lignin during the redox process.[66] The position of this absorbance shifts from 1375 to 1364 cm^{-1} in forward scan and returns to 1374 cm^{-1} in the backward scan. The intensity of this absorbance also increases with applied potential, and decreases following a decrease in potential. The frequency shift and change of peak intensity are related to the conversion of aromatic hydroquinone to non-aromatic quinone moieties.

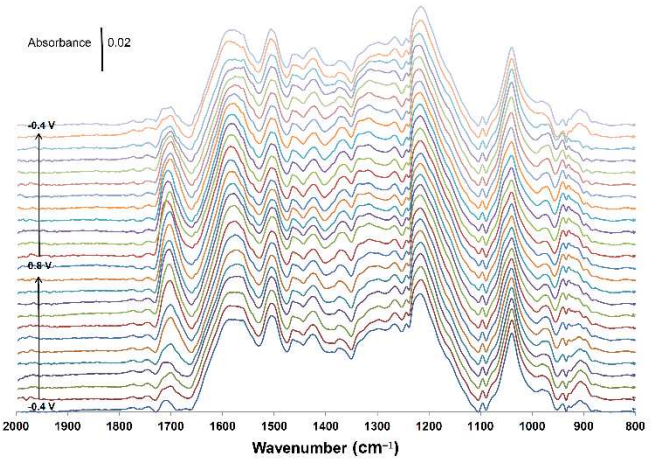

Figure 8. In situ ATR-FTIR spectra of oxidation and reduction of a 1:1 PPy/Lig composite during a complete cycle from -0.4 V to 0.8 V, and returning to -0.4 V, at 1 mV s^{-1} scan rate.

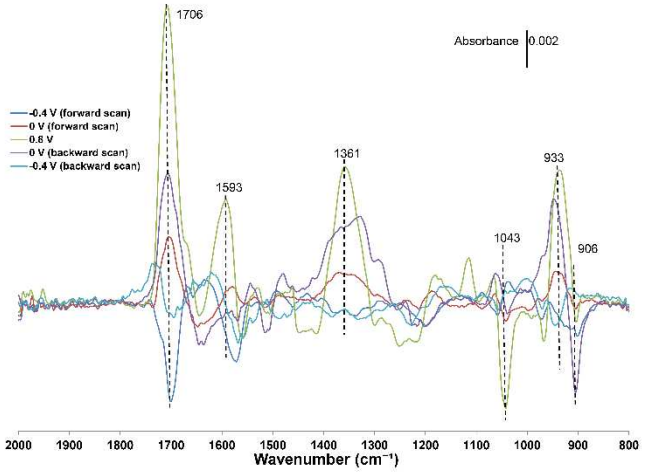

Figure 9. Potential-dependent ATR-FTIR difference spectra of a PPy/Lig composite, showing the same data as in Figure 7, but each spectrum from the in situ experiment was subtracted by the spectrum of the pristine sample. The average of the spectrum from 2000 to 1800 cm^{-1} was used to define the baseline for each curve.

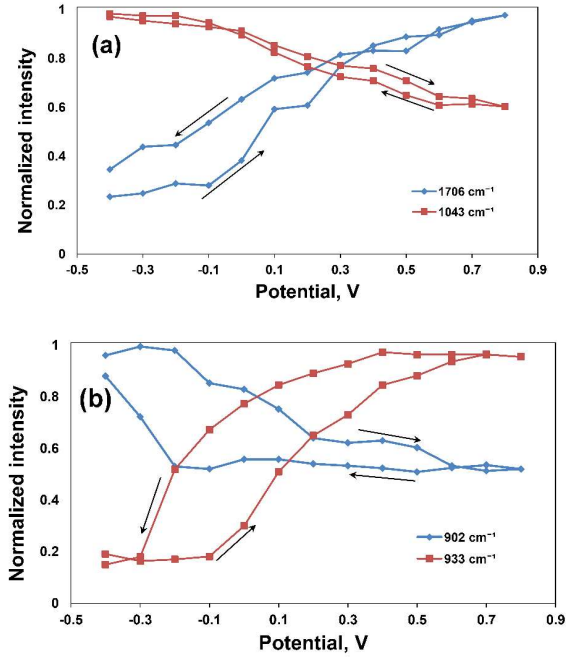

Figure 10. Potential dependence of (a) C=O and C-O vibrational band intensities and (b) different C-H vibrational mode intensities of a 1:1 PPy/Lig composite during a redox cycle. The intensities were obtained via integration over these intervals: 1730-1670 cm^{-1} for C=O, 1070-990 cm^{-1} for C-O, 945-925 cm^{-1} and 920-885 cm^{-1} for the two C-H bands, integrated above a line connecting the interval end points in each spectrum.

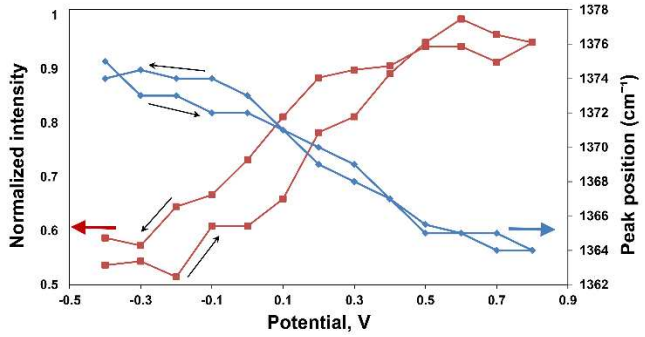

Figure 11. Potential dependence of aromatic/non-aromatic skeletal ring vibrations of lignin during the redox process. The blue curve shows the absorbance shift as a function of applied potential and the red curve shows the normalized intensity of this band at different oxidation states (integrated over 1400-1350 cm^{-1}).

Conclusions

In conclusion, the potential dependence of IR bands during oxidation and reduction demonstrates reversible formation of different redox states in the biocomposite electrodes. *Ex situ* IRAS successfully characterized PPy, lignin and their composites, PPy/Lig structural vibrations were identified and the changes in C=O band intensity was measured at different oxidation states, after 1000 CV and after overoxidation, to show the oxidation and reversibility of the composite. Upon cycling, hydroquinone/quinone conversion occurs in the biopolymer. There are irreversible changes of this biomaterial, visible as carbonyl groups coming from polypyrrole upon overoxidation and long term cycling. Moreover, as a result of overoxidation the quinone redox reaction is no longer observed, as contact between lignin and PPy is cut off due to loss of conduction in PPy. Degradation of polypyrrole leads to formation of soluble products in the electrolyte, which have been identified as maleimide.

By *in situ* ATR-FTIR spectroelectrochemistry, the chemical reactions and structural changes in PPy/Lig composites were studied, and changes of vibrational band intensities and peak positions were examined as a function of applied potential. The reversibility of the *in-situ* IR spectra, with C=O and C-O vibrations at 1706 and 1043 cm^{-1}, confirmed the reversibility of hydroquinone/quinone conversion during the redox process.

Acknowledgements

We thank Luigi Petrone for helpful discussions. This work was supported by the Power Papers project and a Wallenberg Scholar grant to Olle Inganäs from the Knut and Alice Wallenberg foundation, and the Marie Curie network Renaissance. TE acknowledges financial support from the Swedish Government Strategic Research Area in Materials Science on Functional Materials at Linköping University (Faculty Grant SFO-Mat-LiU # 2009-00971). Fatima Nadia

Ajjan and Mohammad Javad Jafari contributed equally to this work.

Notes and references

[a] F.N. Ajjan, Prof. O. Inganäs
Biomolecular and organic electronics
IFM, Linköping University
S-581 83, Linköping, Sweden
E-mail: fataj@ifm.liu.se.com; oling@ifm.liu.se
[b] M.J. Jafari, T. Ederth
Division of Molecular Physics
IFM, Linköping University
S-581 83, Linköping, Sweden
[c] T. Rębiś
Institute of Chemistry and Technical Electrochemistry
Poznan University of Technology
Piotrowo 3, 60–965, Poznan , Poland.

1 R. Dell and D. A. Rand, *J. Power Sources*, 2001, **100**, 2–17.
2 H. Ibrahim, A. Ilinca and J. Perron, *Renew. Sustain. Energy Rev.*, 2008, **12**, 1221–1250.
3 H.-K. Song and G. T. R. Palmore, *Adv. Mater.*, 2006, **18**, 1764–1768.
4 L. Zhao, W. Wang, A. Wang, K. Yuan, S. Chen and Y. Yang, *J. Power Sources*, 2013, **233**, 23–27.
5 H. E. Katz, P. C. Searson and T. O. Poehler, *J. Mater. Res.*, 2010, **25**, 1561–1574.
6 J. F. Mike and J. L. Lutkenhaus, *J. Polym. Sci. Part B Polym. Phys.*, 2013, **51**, 468–480.
7 C. Zhu, J. Zhai, D. Wen and S. Dong, *J. Mater. Chem.*, 2012, **22**, 6300–6306.
8 B. Ding, X. Lu, C. Yuan, S. Yang, Y. Han, X. Zhang and Q. Che, *Electrochimica Acta*, 2012, **62**, 132–139.
9 M. R. Arcila-Velez and M. E. Roberts, *Chem. Mater.*, 2014, **26**, 1601–1607.
10 H. Shirakawa, E. J. Louis, A. G. MacDiarmid, C. K. Chiang and A. J. Heeger, *J. Chem. Soc. Chem. Commun.*, 1977, 578–580.
11 G. Milczarek and O. Inganäs, *Science*, 2012, **335**, 1468–1471.
12 S. Admassie, A. Elfwing, E. W. H. Jager, Q. Bao and O. Inganäs, *J. Mater. Chem. A*, 2014, **2**, 1974–1979.
13 M. Morita, K. Naoi, *The Electrochemical Society Interface,* 2008*,* **17**, 44–48.
14 P. Novák, K. Müller, K. S. V. Santhanam and O. Haas, *Chem. Rev.*, 1997, **97**, 207–282.
15 L. Nyholm, G. Nyström, A. Mihranyan and M. Strømme, *Adv. Mater.*, 2011, **23**, 3751–3769.
16 G. Nystrom, A. Mihranyan, A. Razaq, T. Lindstrom, L. Nyholm and M. Strømme, *J. Phys. Chem. B*, 2010, **114**, 4178–4182.
17 B. Scrosati, *Nat. Nanotechnol.*, 2007, **2**, 598–599.
18 H. Olsson, D. O. Carlsson, G. Nyström, M. Sjödin, L. Nyholm and M. Strømme, *J. Mater. Sci.*, 2012, **47**, 5317–5325.
19 P. Novák, O. Inganäs and R. Bjorklund, *J. Electrochem. Soc.*, 1987, **134**, 1341–1345.
20 P. Novák, O. Inganäs and R. Bjorklund, *J. Power Sources*, 1987, **21**, 17–24.
21 J. Rencoret, A. Gutiérrez, L. Nieto, J. Jiménez-Barbero, C. B. Faulds, H. Kim, J. Ralph, Á. T. Martínez and J. C. del Río, *Plant Physiol.*, 2011, **155**, 667–682.
22 G. Milczarek, *Langmuir*, 2009, **25**, 10345–10353.
23 G. Milczarek, *Electroanalysis*, 2008, **20**, 211–214.
24 L. Dunsch, *J. Solid State Electrochem.*, 2011, **15**, 1631–1646.
25 A. Šurca, B. Orel, G. Dražič and B. Pihlar, *J. Electrochem. Soc.*, 1999, **146**, 232–242.
26 P. Damlin, C. Kvarnström and A. Ivaska, *J. Electroanal. Chem.*, 2004, **570**, 113–122.
27 C. Kvarnström, H. Neugebauer, S. Blomquist, H. J. Ahonen, J. Kankare and A. Ivaska, *Electrochimica Acta*, 1999, **44**, 2739–2750.
28 P. A. Christensen and A. Hamnett, *Electrochimica Acta*, 1991, **36**, 1263–1286.
29 D. J. Fermín, H. Teruel and B. R. Scharifker, *J. Electroanal. Chem.*, 1996, **401**, 207–214.
30 Y. Furukawa, S. Tazawa, Y. Fujii and I. Harada, *Synth. Met.*, 1988, **24**, 329–341.
31 S. Lamprakopoulos, D. Yfantis, A. Yfantis, D. Schmeisser, J. Anastassopoulou and T. Theophanides, *Synth. Met.*, 2004, **144**, 229–234.
32 G. I. Mathys and V.-T. Truong, *Synth. Met.*, 1997, **89**, 103–109.
33 S. Ghosh, G. A. Bowmaker, R. P. Cooney and J. M. Seakins, *Synth. Met.*, 1998, **95**, 63–67.
34 I. Rodríguez, B. R. Scharifker and J. Mostany, *J. Electroanal. Chem.*, 2000, **491**, 117–125.
35 H. Xie, M. Yan and Z. Jiang, *Electrochimica Acta*, 1997, **42**, 2361–2367.
36 M. Kofranek, T. Kovář, A. Karpfen and H. Lischka, *J. Chem. Phys.*, 1992, **96**, 4464–4473.
37 R. Kostić, D. Raković, S. A. Stepanyan, I. E. Davidova and L. A. Gribov, *J. Chem. Phys.*, 1995, **102**, 3104–3109.
38 B. Tian and G. Zerbi, *J. Chem. Phys.*, 1990, **92**, 3886–3891.
39 B. Tian and G. Zerbi, *J. Chem. Phys.*, 1990, **92**, 3892–3898.
40 U. Agarwal and R. Atalla, in *Lignin and Lignans*, eds. C. Heitner, D. Dimmel and J. Schmidt, CRC Press, 2010, pp. 103–136.
41 A. P. Karmanov and O. Y. Derkacheva, *Russ. J. Bioorganic Chem.*, 2013, **39**, 677–685.
42 O. Derkacheva and D. Sukhov, *Macromol. Symp.*, 2008, **265**, 61–68.
43 *Holzforschung*, 1997, **51**, 167–168.
44 UmeshP Agarwal and RajaiH Atalla, in *Lignin and Lignans*, CRC Press, 2010, pp. 103–136.
45 H. L. Hergert, *J. Org. Chem.*, 1960, **25**, 405–413.
46 W. E. Collier, T. P. Schultz and V. F. Kalasinsky, *Holzforschung*, 1992, **46**, 523–528.
47 S. Detoni and D. Hadzi, *Spectrochim. Acta*, 1956, **11**, 601–608.
48 J. Lei and C. R. Martin, *Synth. Met.*, 1992, **48**, 331–336.
49 M. Bazzaoui, L. Martins, E. A. Bazzaoui and J. I. Martins, *J. Electroanal. Chem.*, 2002, **537**, 47–57.
50 J. Lei, W. Liang and C. R. Martin, *Synth. Met.*, 1992, **48**, 301–312.
51 A. Kaynak, L. Rintoul and G. A. George, *Mater. Res. Bull.*, 2000, **35**, 813–824.
52 J. Suárez-Guevara, O. Ayyad and P. Gómez-Romero, *Nanoscale Res. Lett.*, 2012, **7**, 1–6.
53 N. Hassanzadeh, H. Omidvar and S. H. Tabaian, *Superlattices Microstruct.*, 2012, **51**, 314–323.
54 N. Strand, A. Bhushan, M. Schivo, N. J. Kenyon and C. E. Davis, *Sens. Actuators B Chem.*, 2010, **143**, 516–523.
55 C. Arribas and D. Rueda, *Synth. Met.*, 1996, **79**, 23–26.
56 N. V. Bhat, A. P. Gadre and V. A. Bambole, *J. Appl. Polym. Sci.*, 2003, **88**, 22–29.
57 J. F. Rabolt, T. C. Clarke and G. B. Street, *J. Chem. Phys.*, 1979, **71**, 4614.
58 C. G. Boeriu, D. Bravo, R. J. A. Gosselink and J. E. G. van Dam, *Ind. Crops Prod.*, 2004, **20**, 205–218.
59 T. W. Lewis, G. M. Spinks, G. G. Wallace, A. Mazzoldi and D. De Rossi, *Synth. Met.*, 2001, **122**, 379–385.
60 Y. Li and R. Qian, *Electrochimica Acta*, 2000, **45**, 1727–1731.
61 C. Debiemme-Chouvy and T. T. M. Tran, *Electrochem. Commun.*, 2008, **10**, 947–950.
62 D.-S. Park, Y.-B. Shim and S.-M. Park, *J. Electrochem. Soc.*, 1993, **140**, 609–614.
63 D.-S. Park, Y.-B. Shim and S.-M. Park, *J. Electrochem. Soc.*, 1993, **140**, 2749–2752.
64 J. C. Thiéblemont, J. L. Gabelle and M. F. Planche, *Synth. Met.*, 1994, **66**, 243–247.
65 J.-L. Wen, B.-L. Xue, F. Xu, R.-C. Sun and A. Pinkert, *Ind. Crops Prod.*, 2013, **42**, 332–343.
66 G. Milczarek, *Electroanalysis*, 2007, **19**, 1411–1414.

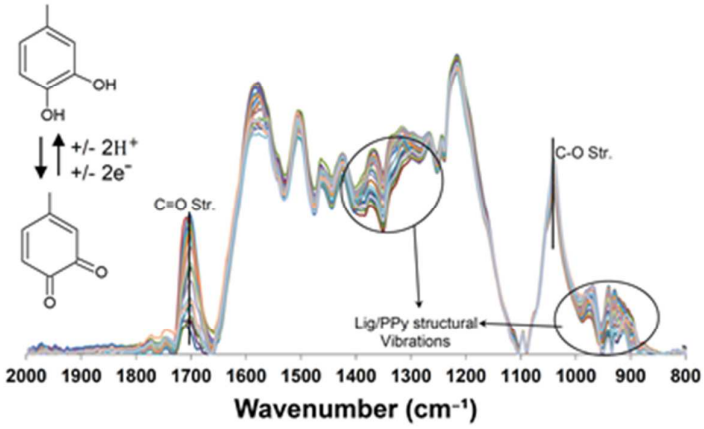

Spectroelectrochemical Investigation of Redox States in a Polypyrrole/Lignin Composite Electrode Material.